

# Geophysical Research Letters®



## RESEARCH LETTER

10.1029/2024GL111839

## Slow-to-Fast Transition and Shear Localization in Accelerating Creep of Clayey Soil

### Special Collection:

Slow to fast earthquakes and the geology, structure, and rheology of their host subduction zones

Chengrui Chang<sup>1,2</sup> , Hiroyuki Noda<sup>3</sup> , Qiang Xu<sup>2</sup> , Dongliang Huang<sup>4</sup> , and Tetsuo Yamaguchi<sup>1</sup>

Chengrui Chang, visiting scholar at <sup>2</sup> SKLGP.

<sup>1</sup>Department of Biomaterial Sciences, Graduate School of Agricultural and Life Sciences, The University of Tokyo, Tokyo, Japan, <sup>2</sup>State Key Laboratory of Geohazard Prevention and Geo-environment Protection, Chengdu University of Technology, Chengdu, China, <sup>3</sup>Disaster Prevention Research Institute, Kyoto University, Uji, Japan, <sup>4</sup>Previously at School of Civil Engineering, Central South University, Changsha, China

### Key Points:

- Fluid-injection creep experiments on clayey soil show two distinct acceleration regimes, with a dynamic transition based on shear history
- The regularized rate-and-state friction model describes the power-law velocity-acceleration relationships and exponents for both regimes
- The model, coupled with idealized shear localization in a multilayer structure, qualitatively reproduces the history-dependent transitions

### Supporting Information:

Supporting Information may be found in the online version of this article.

### Correspondence to:

T. Yamaguchi and Q. Xu, [yamaguchi-tetsuo@g.ecc.u-tokyo.ac.jp](mailto:yamaguchi-tetsuo@g.ecc.u-tokyo.ac.jp); [xq@cdut.edu.cn](mailto:xq@cdut.edu.cn)

### Citation:

Chang, C., Noda, H., Xu, Q., Huang, D., & Yamaguchi, T. (2024). Slow-to-fast transition and shear localization in accelerating creep of clayey soil. *Geophysical Research Letters*, 51, e2024GL111839. <https://doi.org/10.1029/2024GL111839>

Received 6 AUG 2024

Accepted 22 NOV 2024

### Author Contributions:

**Conceptualization:** Chengrui Chang, Hiroyuki Noda, Qiang Xu, Dongliang Huang, Tetsuo Yamaguchi  
**Data curation:** Chengrui Chang  
**Formal analysis:** Chengrui Chang, Hiroyuki Noda, Tetsuo Yamaguchi

**Abstract** Accelerating creep before catastrophic failure commonly follows a power-law velocity-acceleration relationship, with the exponent typically near 2 but often evolving from 1 to 2 at a certain point, indicating a dynamic transition. The underlying mechanisms, however, remain unclear. Here we investigate this transition by monitoring the slip displacement of clayey soil during fluid-injection creep experiments. This transition is discontinuous in the first run but becomes continuous in the initially pre-sheared sample. Using a regularized rate-and-state friction model, we explicitly examine the relationship between the exponent and the frictional properties of the soil. This model describes the dynamic transition, with the exponent evolving from 1 to 2 across a broad range of frictional parameters. Furthermore, by incorporating idealized shear localization processes, the model qualitatively reproduces the shear-history-dependent transition. Our study demonstrates that a combination of structural evolutions and frictional properties may explain slow and fast slips observed in various shear systems.

**Plain Language Summary** Predicting when materials will fail or natural hazards will occur is complex because it involves various physical processes and parameters. An empirical power-law velocity-acceleration relationship has proven effective and reliable for forecasting creep failure and natural events like landslides and volcanic eruptions. Although its exponent is typically 2, it can evolve from 1 to 2 over time, indicating a dynamic transition between two distinct acceleration regimes. In our fluid-injection experiments on clayey soil, we observe a slow-to-fast transition in slip displacement and a multi-layered shear zone. This transition is initially discontinuous but becomes continuous when the sample is pre-sheared. To elucidate the mechanism, we use a slider block to simplify landslide movement, with the friction of the slip surface governed by a regularized rate-and-state friction model. For a velocity-weakening slip surface, this model predicts a shift from velocity-independent to velocity-weakening steady-state friction, demonstrating a continuous slow-to-fast transition with the exponent evolving from 1 to 2. Furthermore, the combination of friction and shear localization processes qualitatively reproduces the discontinuous transition observed in experiments. These results indicate that slow and fast slips can be modulated by both frictional property and structural evolution, encouraging the consideration of their combined effects.

## 1. Introduction

Natural instability phenomena, including landslides and volcanic eruptions, have been quantified by an empirical scaling law relating the deformation rate  $\dot{\Omega}$  and its acceleration  $\ddot{\Omega}$  as

$$\ddot{\Omega} = A\dot{\Omega}^\alpha, \quad (1)$$

where  $\Omega$  is the measurable deformation such as surface displacement, the dot represents time derivative, and  $A$  and  $\alpha$  are empirical parameters. This law was discovered in slope-failure experiments by Fukuzono (1985) and subsequently applied to other systems (e.g., Main, 1999; Voight, 1988, 1989), often referred to as the Voight model (e.g., Federico et al., 2012; Intrieri et al., 2019). In practice, this empirical relationship exhibits striking yet not fully understood generality and has proven robust in predicting failure across various geological settings (e.g., Rose & Hungr, 2007; Sornette et al., 2004; Voight, 1989) and experiments under constant or monotonic loading conditions (e.g., Chang & Wang, 2022; Fukuzono, 1985; Heap et al., 2011; Xue et al., 2018). For instance, if  $\Omega$

© 2024. The Author(s).

This is an open access article under the terms of the Creative Commons Attribution License, which permits use, distribution and reproduction in any medium, provided the original work is properly cited.

**Funding acquisition:** Chengrui Chang, Tetsuo Yamaguchi  
**Investigation:** Chengrui Chang, Dongliang Huang  
**Supervision:** Tetsuo Yamaguchi  
**Writing – original draft:** Chengrui Chang  
**Writing – review & editing:** Hiroyuki Noda, Qiang Xu, Dongliang Huang, Tetsuo Yamaguchi

represents slip displacement in a localized shear zone, a landslide would show a proportional relationship between the logarithm of creep acceleration and the logarithm of creep velocity near failure.

This proportionality is characterized by the exponent  $\alpha$  (Equation 1), which typically lies between 1 and 2, frequently close to 2 (e.g., Segalini et al., 2018; Voight, 1989). Nevertheless, it can vary, as seen in seasonal landslide accelerations (Crosta & Agliardi, 2003), and tends to increase from 1 to 2 in volcanic eruptions (e.g., Kilburn, 2003; McGuire & Kilburn, 1997) and landslides (e.g., Hayashi & Yamamori, 1991), indicating a slow-to-fast dynamic transition between two acceleration regimes. Examples include the September 1981 eruption at Mt. St. Helens (McGuire & Kilburn, 1997; Voight, 1988) and the 1962 Vaiont landslide movement event (D. Petley and Petley, 2006). Moreover, significantly small  $\alpha$  values have been observed in landslides (Bozzano et al., 2014) and volcanic activities (Tepp et al., 2020).

The rate- and state-dependent friction (RSF) laws (Dieterich, 1979; Ruina, 1983), widely used in fault mechanics (e.g., Marone, 1998), have been applied to model accelerating creep of landslides as a slider block under constant loading, predicting  $\alpha = 2$  (Helmstetter et al., 2004; Noda & Chang, 2023). Field and experimental observations suggest that variable  $\alpha$  values may result from changes in deformation mechanisms and structural evolution (Chang & Wang, 2022; Petley et al., 2002), implying the role of deformation history. In this article, we build on previous experiments and analyses to examine the mechanism behind the evolving  $\alpha$  and the role of structural evolution.

## 2. Experiment

### 2.1. Experimental Setup

We conducted fluid-injection shear experiments to simulate rain-induced landslides on clayey soil with slope angle  $\varphi$ , using elevated pore pressure  $P$ , as depicted by the schematic in Figure 1a. Extending upon the method in Chang and Wang (2022), we used the same ring-shear configuration (Figure 1b) and clayey soil (see Expanded Methods and Figure S1 in Supporting Information S1). The soil, taken from a landslide, was sieved to remove particles larger than 4.75 mm for experimentation. It primarily comprises highly weathered schist, containing minerals such as quartz, mica, chlorite, and illite, with approximately 20% clay content. Dry, sieved samples were evenly placed in the configuration shown in Figure 1b, water-saturated, and preconditioned with a constant normal stress  $\sigma_0$  of 200 kPa and shear stress  $\tau_0$  to simulate slope stress conditions (Table S1 in Supporting Information S1). Specifically, the configuration dictates concentrated shear deformation between its stationary and rotary parts, allowing us to repeat the same preconditioning and experimental protocol, thereby naturally introducing a pre-existing shear zone into the sample. Pore pressure  $P$  is measured through a porous metal component positioned slightly higher than the shear box separation. Sample height change  $\Delta h$  is recorded by a vertical displacement sensor attached to the loading ring.

Pore pressure  $P$  was then increased linearly by a pressure intensifier, with sample dilation observed concurrently (Figures 1b and 1c), while  $\sigma_0$  and  $\tau_0$  were kept constant until failure marked by evident decreases in  $\tau$  (Figure 1c). Consequently, slip displacement  $\delta$ , equivalent to  $\Omega$  in Equation 1, increased, showing accelerating velocity  $\dot{\delta}$ . A quasi-static condition,  $\tau_0 = \rho g \sin \varphi$  (where  $\rho$  and  $g$  are density and gravitational acceleration, respectively), is maintained before failure, with acceleration  $\ddot{\delta} \ll g \sin \varphi$ , despite the rate of pore pressure increase  $\dot{P}$  ranging from 30 to 120 kPa/hr (Table S1 in Supporting Information S1). Accelerating creep is defined from the onset of acceleration to the failure point, corresponding to  $\delta_0$  and  $\delta_f$ , respectively (dashed lines in Figure 1c). A large  $\delta_0$  thus indicates substantial pre-shearing of the sample (Figure 1c, right panels). Additionally, we incorporate the fluid-injection experiments in Chang and Wang (2022) into our analysis (Table S1 in Supporting Information S1).

### 2.2. Slow-To-Fast Transition and Shear Localization

Figure 2 presents representative results of acceleration versus velocity in log-log plots. Velocity and acceleration are derived from filtered time-displacement data for clarity (see Expanded Analyses and Figure S2 in Supporting Information S1). For the sample undergoing first-time shear (Figure 2a), two distinct acceleration regimes are observed, characterized by a slow-to-fast transition with a stepwise increase in  $\alpha$  from 1 to 2. During this

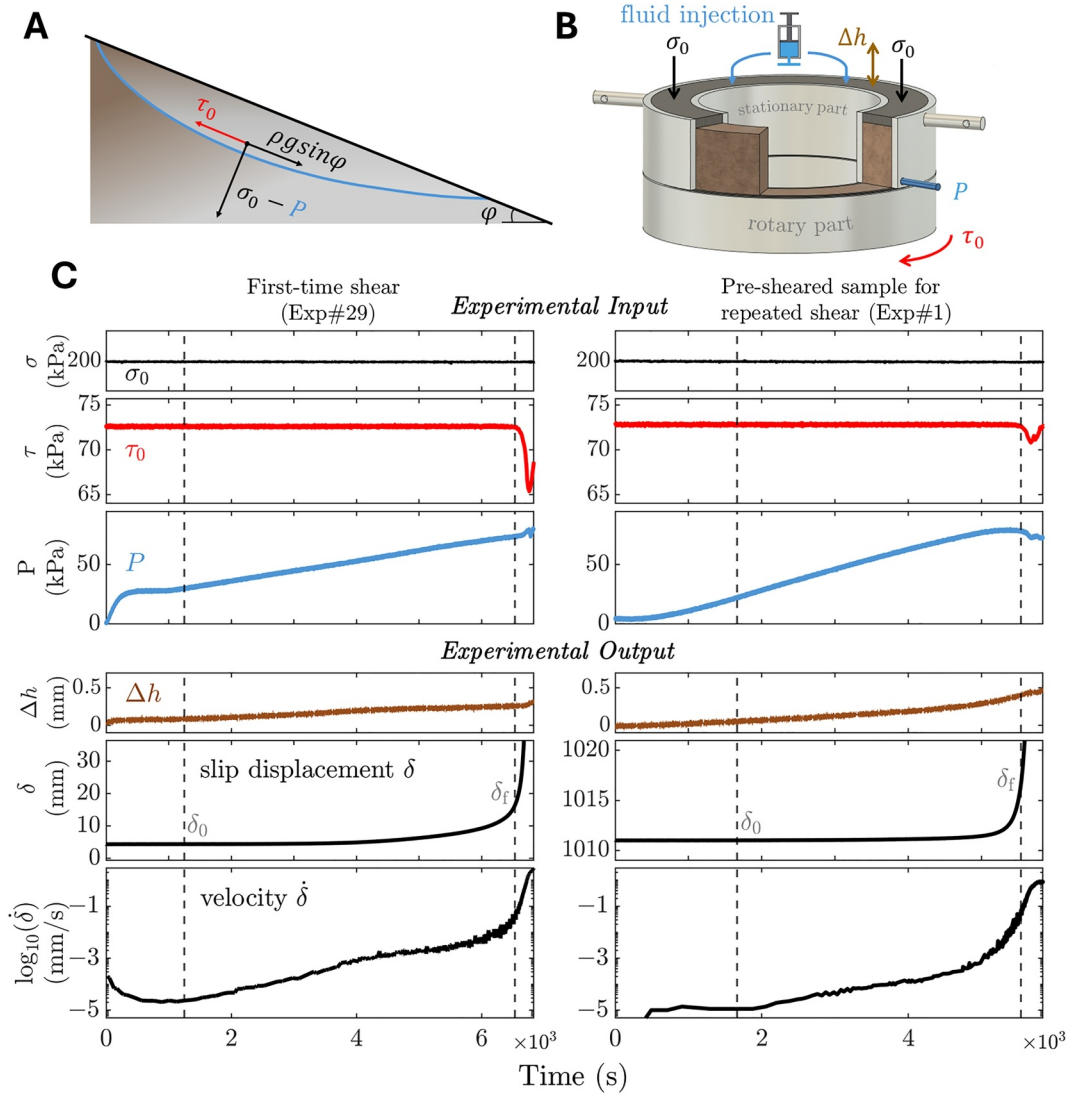


**Figure 1.** Schematics for the landslide model (a) and experimental setup (b). Representative input and output measurements (c) for the first-time shear (left) and repeated shear (right) experiments (Dashed lines indicate periods of accelerating creep).

transition, the curve temporarily deviates from the power-law relationship, showing a dip as transient decreases in acceleration. In contrast, the pre-sheared sample under repeated shear shows a continuous transition without the dip (Figure 2b), where  $\alpha$  increases to a value smaller than 2, possibly due to the reduced pore pressure within the pre-existing shear zone accompanied by dilation (Figure 1c, right panels; Expanded Analyses in Supporting Information).

We summarize the slip displacement during accelerating creep,  $\delta_A = \delta_f - \delta_0$ , from all experiments (Table S1 in Supporting Information S1). Notably,  $\delta_A$  exhibits significantly reduced variability when  $\delta_0$  is large (Figure 3a), suggesting the influence of shear history. To illustrate this pre-sheared deformation, we present pictures of a sample with  $\sim 2$  m displacement in Figure 3b, revealing a  $\sim 1$  cm thick shear zone within unsheared soil. Close-ups of the shear zone feature slickenlines on its boundaries and foliation with multilayer structures within the cross-section.

Hence, we propose two questions to address the above observations: What is the mechanism for the observed slow-to-fast transition? And why does the dip occur in the samples subjected to first-time shear?

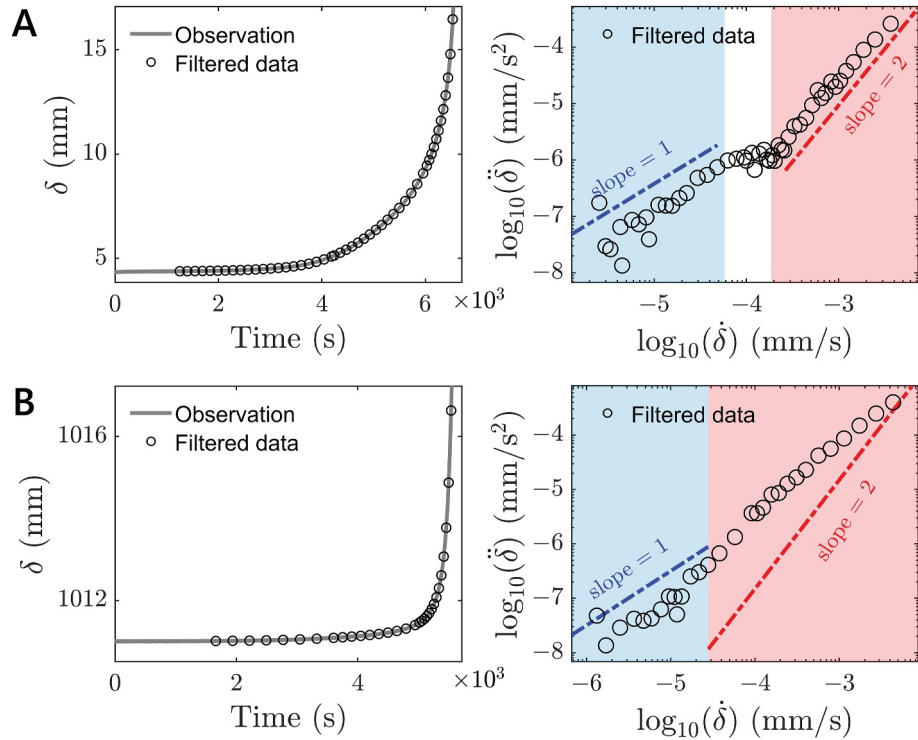


**Figure 2.** Time-displacement curves and log-log plots for acceleration versus velocity from representative experiments: Sample undergoing the first-time shear (a) and pre-sheared sample subjected to repeated shear (b) (Dashed lines with slopes of 1 and 2 serve as guides to the eye).

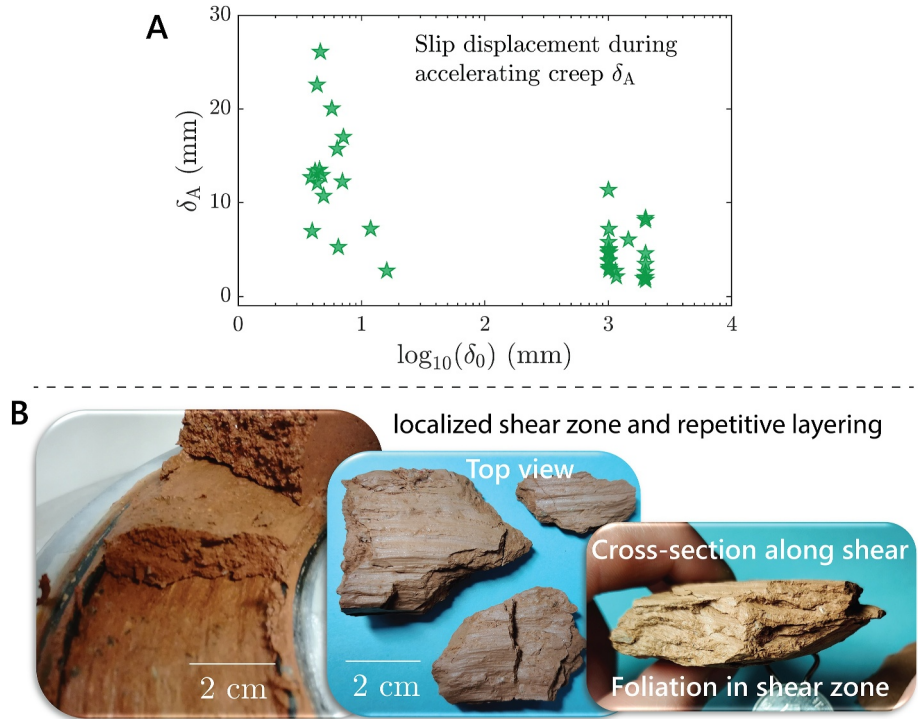


**Figure 3.** The distribution of accelerating creep displacement  $\delta_A$  versus  $\delta_0$  (a) from experiments. Pictures of a sample with  $\sim 2$  m slip displacement, including close-ups of the top view and cross-section of the shear zone.

### 3. Single Slip Surface Model

#### 3.1. Regularized Rate-and-State Friction (RSF) Model

We begin by extending upon the theory of the accelerating creep with RSF proposed by Noda and Chang (2023). The RSF law captures both the instantaneous response of the friction coefficient to a change in slip velocity, termed the direct effect, and the subsequent longer-term relaxation process, referred to as the evolution effect. A typical formula expresses the friction coefficient of a slip surface as

$$f(V, \theta) = f_* + a \ln\left(\frac{V}{V_*}\right) + b \ln\left(\frac{\theta}{\theta_*}\right), \quad (2)$$

where  $V$  is the slip velocity,  $\theta$  is the state variable representing the evolving state of the surface, and  $a$  and  $b$  are nondimensional parameters that characterize the direct and evolution effects, respectively. A reference state is arbitrarily selected at  $V_*$ ,  $\theta_* = L/V_*$ , and  $f_* = f(V_*, \theta_*)$ .

The state-evolution equation describes the time derivative of  $\theta$  in terms of  $V$  and  $\theta$  (Ruina, 1983) and many equation forms have been proposed (e.g., Marone, 1998). Here we adopt the commonly used aging law and slip law (Ruina, 1983):

$$\frac{d\theta}{dt} = \begin{cases} 1 - \frac{V\theta}{L} & (\text{Aging law}), \\ -\frac{V\theta}{L} \ln\left(\frac{V\theta}{L}\right) & (\text{Slip law}), \end{cases} \quad (3)$$

where  $L$  is the characteristic slip displacement for state evolution. The steady-state condition  $d\theta/dt = 0$  leads to  $\theta_{ss} = L/V$ , which results in the steady-state friction coefficient as

$$f_{ss} = f_* + (a - b) \ln\left(\frac{V}{V_*}\right). \quad (4)$$

We focus on the instability of rain-induced landslides that are initially at rest or slipping slowly until a sufficient pore pressure increment is imposed (Figure 1). However, a “stop” state ( $V = 0$ ) is not defined in Equation 2 because of the divergence of the logarithm when  $V \rightarrow 0$ . Following the rate-dependent plasticity model of Drysdale (1984) and Drysdale and Zak (1985), this term vanishes at  $V = 0$  in a purely elastic regime, yielding a stress level that represents a “stop” condition. Similarly, a regularized RSF model proposed by Andrés et al. (2019) can naturally define stationary conditions by introducing a threshold velocity  $V_{th}$  and a corresponding state  $\theta_{th} = L/V_{th}$  and friction level  $f_0 = f(V_{th}, \theta_{th})$  into Equation 2 as:

$$f(V, \theta) = f_0 + a \ln\left(\frac{V + V_{th}}{V_{th}}\right) + b \ln\left(\frac{\theta}{\theta_{th}}\right), \quad (5)$$

The state-evolution equations (Equation 3) are regularized to

$$\frac{d\theta}{dt} = \begin{cases} 1 - \frac{(V + V_{th})\theta}{L} & (\text{Aging law}), \\ -\frac{(V + V_{th})\theta}{L} \ln\left[\frac{(V + V_{th})\theta}{L}\right] & (\text{Slip law}). \end{cases} \quad (6)$$

This regularization is equivalent to the models in Yang et al. (2008), Tal et al. (2018), and Paul et al. (2024). It recovers conventional RSF (Equations 2–4) when  $V \gg V_{th}$ , but behaves differently at small velocities; more precisely, the frictional responses become independent of  $V$  at infinitesimal velocity ( $V \ll V_{th}$ ).  $\theta_{ss} = L/(V + V_{th})$  satisfies the steady state, leading to the steady-state friction coefficient:

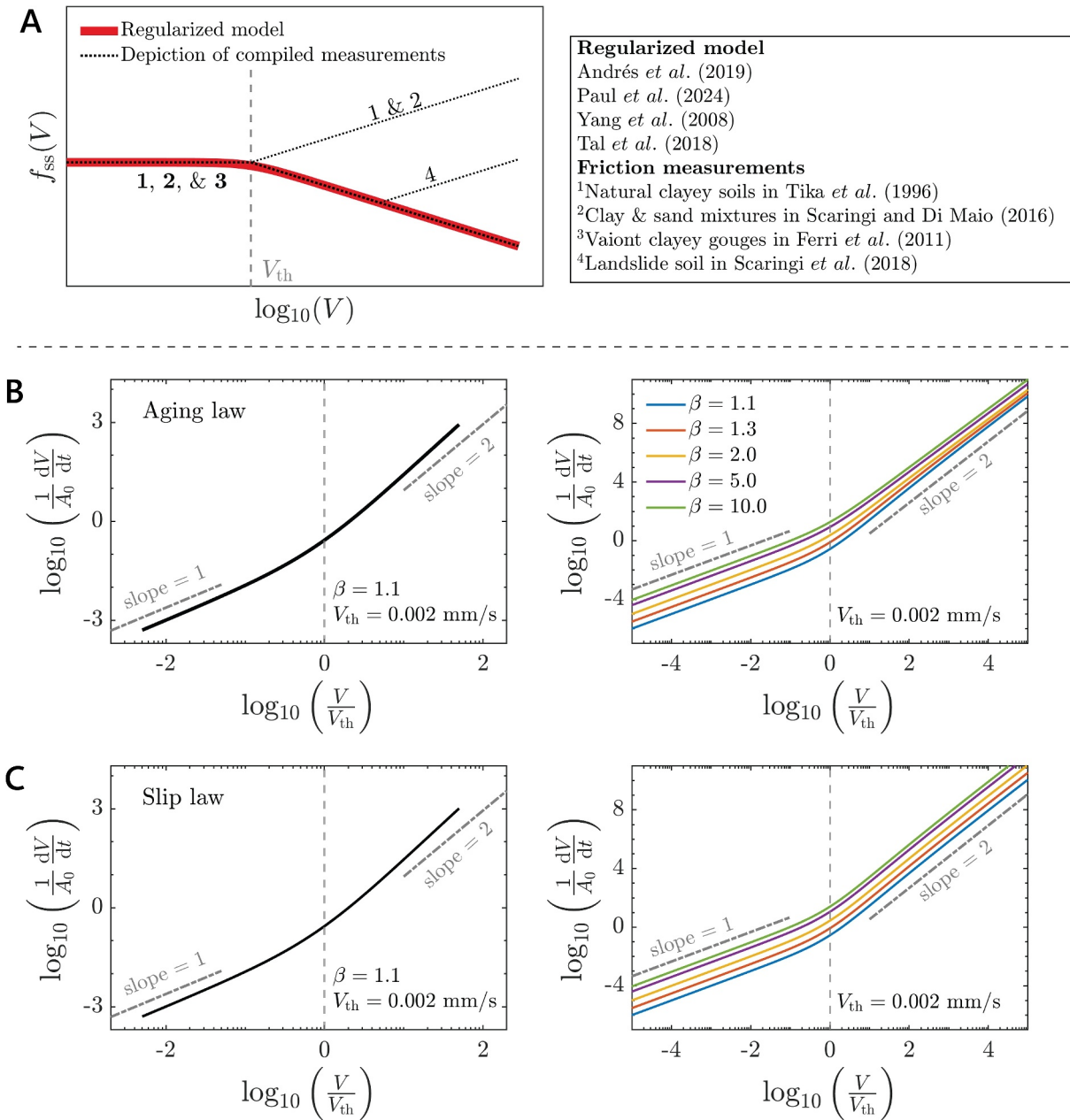


**Figure 4.** Compiled friction data of clayey soil from literature overlaid with the regularized RSF model for a velocity-weakening slip surface (a). Nondimensional acceleration  $1/A_0 \cdot dV/dt$  versus nondimensional velocity  $V/V_{th}$  for the single slip surface model in the aging law (b) and slip law (c) (Dashed lines with slopes of 1 and 2 serve as guides to the eye).

$$f_{ss} = f_0 + (a - b) \ln\left(\frac{V + V_{th}}{V_{th}}\right). \quad (7)$$

Thus,  $df_{ss}/d \ln(V) = V/(V + V_{th})(a - b)$  determines stability. Positive  $a - b$ , referred to as velocity-strengthening, indicates a stable system, as friction increases with velocity. Conversely, we use negative  $a - b$  to characterize a velocity-weakening shear zone that can potentially accelerate catastrophically, the steady-state friction (Equation 7) for which is illustrated in Figure 4a, where  $f_{ss}$  asymptotically approaches  $f_0$  when  $V < V_{th}$ .

Data compiled from ring-shear tests on various soils (Scaringì & Di Maio, 2016; Tika et al., 1996) show velocity-independent steady-state friction at small velocities, typically less than  $V_{th} \approx 0.002$  mm/s (Figure 4a). These measurements, often obtained from substantially pre-sheared samples, suggest the friction properties of a localized slip surface. As the velocity increases, some clayey soils exhibit velocity-weakening behavior while others show velocity-strengthening. Interestingly, the clayey gouges from the Vaiont landslide show a transition from velocity-independent to velocity-weakening friction (Ferri et al., 2011). The next section will apply the regularized model that captures this transition in various clayey soils. Data from Scaringì et al. (2018) also suggest a second threshold velocity leading to velocity-strengthening, although this aspect falls beyond the scope of our study.

### 3.2. Accelerating Creep for Regularized Model

We now adopt the regularized model to analyze the initiation of catastrophic acceleration from  $V = 0$  under quasi-static conditions. For simplicity, we assume a constant-load condition and neglect both inertia and any pore-pressure variations. Unlike the selection of reference  $V_*$  and  $\theta_*$  in conventional RSF, a reference state here is defined by  $V = 0$ ,  $\theta_{th} = L/V_{th}$  and  $f_0 = f(V = 0, \theta_{th})$ . This approach simplifies equations, enabling a constant friction level  $f = f_0$  for creep tests without any loss of generality. Consequently, Equation 5 reduces to

$$a \ln\left(\frac{V + V_{th}}{V_{th}}\right) + b \ln\left(\frac{\theta}{\theta_{th}}\right) = 0. \quad (8)$$

For brevity, we denote a frictional parameter  $\beta = b/a$  and Equation 8 becomes

$$\frac{V}{V_{th}} = \left(\frac{\theta}{\theta_{th}}\right)^{-\beta} - 1. \quad (9)$$

The time derivative of Equation 9 leads to the acceleration:

$$\frac{dV}{dt} = \frac{V_{th}^2}{L} \left[ -\beta \left( \frac{V}{V_{th}} + 1 \right)^{\frac{1+\beta}{\beta}} \right] \frac{d\theta}{dt}. \quad (10)$$

Equation (10) resembles the Voight model (Equation 1) and indicates that  $\alpha$  may depend on  $\beta$  and the evolution-equation  $d\theta/dt$ . Substituting state-evolution equations (Equation 6) into Equation (10) gives the acceleration as

$$\frac{dV}{dt} = \begin{cases} \frac{V_{th}^2}{L} \left\{ \beta \left( \frac{V}{V_{th}} + 1 \right)^2 \left[ 1 - \left( \frac{V}{V_{th}} + 1 \right)^{-\frac{\beta-1}{\beta}} \right] \right\} \text{(Aging law),} \\ \frac{V_{th}^2}{L} \left[ (\beta - 1) \left( \frac{V}{V_{th}} + 1 \right)^2 \ln\left( \frac{V}{V_{th}} + 1 \right) \right] \text{(Slip law).} \end{cases} \quad (11)$$

For brevity, we denote  $A_0 = V_{th}^2/L$  and use  $V/V_{th}$  to represent nondimensional velocity. Nondimensional acceleration is therefore  $1/A_0 \cdot dV/dt$ , as indicated by the terms in brackets in Equation (11).

For a velocity-weakening slip surface (where  $\beta > 1$ ), Equation 11 indicates accelerating creep, where  $dV/dt > 0$  for  $V > 0$ . We use  $\beta = 1.1$  and the typical  $V_{th} = 0.002$  mm/s (Figure 4a) as an example and adopt  $10^{-5} < V < 10^{-1}$  mm/s, a typical velocity range in experiments (Figure 2), for the analysis. The slow-to-fast transition between two distinct acceleration regimes, with  $\alpha$  evolving from 1 to 2, is shown in the log-log plots of nondimensional acceleration versus nondimensional velocity for both the aging law and slip law (Figures 4b and 4c, left panels). Subsequently, we incorporate  $1 < \beta \leq 10$  (Noda & Chang, 2023) and find that  $\alpha$  is insensitive to  $\beta$  values (Figures 4b and 4c, right panels).

We then evaluate the value of  $\alpha$ . The Taylor series for Equation 11 around  $V = 0$  is given by

$$\frac{1}{A_0} \frac{dV}{dt} = \begin{cases} (\beta - 1) \frac{V}{V_{th}} + O(V^2) \text{ (Aging law)}, \\ (\beta - 1) \frac{V}{V_{th}} + O(V^2) \text{ (Slip law)}, \end{cases} \quad (12)$$

indicating  $\alpha = 1$  when  $V \ll V_{th}$ . When  $V \gg V_{th}$ , the approximate equation is

$$\frac{1}{A_0} \frac{dV}{dt} = \begin{cases} \beta \left(\frac{V}{V_{th}}\right)^2 \text{ (Aging law)}, \\ C(\beta - 1) \left(\frac{V}{V_{th}}\right)^2 \text{ (Slip law)}, \end{cases} \quad (13)$$

where  $C$  is a numerical constant on the order of 1 for the range of  $V$  in our experiments. Compared to the Voight model (Equation 1), Equation 13 suggests that  $\alpha$  converges to 2 for  $V \gg V_{th}$ , consistent with Noda and Chang (2023) for conventional RSF. In summary,  $\alpha$  is

$$\alpha = \begin{cases} 1, & V \ll V_{th}, \\ 2, & V \gg V_{th}. \end{cases} \quad (14)$$

Thus, the shift from velocity-independent to velocity-weakening behavior is a key mechanism driving the stepwise increase of  $\alpha$  from 1 to 2, with potential general applicability across various soil types (Figure 4a).

#### 4. Model With Shear Localization

The analysis above assumes a single slip surface, whereas images of the shear zone (Figure 3b) show significant structural evolution before a single slip surface is well-formed. The shear zone comprises multiple interconnected layers that accommodate slip displacement. To simplify this multilayer structure, we introduce an idealized number of active layers,  $N$ . For a sample experiencing first-time shear,  $N$  is large initially, while a substantially pre-sheared sample has  $N = 1$ . The observed velocity  $V$  is thus the sum of the slip velocities from  $N$  layers, each assumed to share the same velocity  $V/N$ . We incorporate this concept into Equation 5 as

$$f\left(\frac{V}{N}, \theta\right) = f_0 + a \ln\left(\frac{\frac{V}{N} + V_{th}}{V_{th}}\right) + b \ln\left(\frac{\theta}{\theta_{th}}\right). \quad (15)$$

The state-evolution equation becomes

$$\frac{d\theta}{dt} = \begin{cases} 1 - \frac{\left(\frac{V}{N} + V_{th}\right)\theta}{L} \text{ (Aging law)}, \\ -\frac{\left(\frac{V}{N} + V_{th}\right)\theta}{L} \ln\left[\frac{\left(\frac{V}{N} + V_{th}\right)\theta}{L}\right] \text{ (Slip law)}. \end{cases} \quad (16)$$

We continue with the same friction level and the reference state  $f_0 = f(V = 0, \theta_{th})$  for creep tests. Consequently, Equation 15 simplifies to

$$\frac{V}{V_{th}} = N \left[ \left( \frac{\theta}{\theta_{th}} \right)^{-\beta} - 1 \right]. \quad (17)$$

The time derivative of Equation 17 gives the acceleration:

$$\frac{dV}{dt} = A_0 \left[ \frac{dN}{dt} \frac{V}{N} \frac{L}{V_{th}^2} - \beta N \left( \frac{V}{V_{th}N} + 1 \right)^{\frac{1+\beta}{\beta}} \frac{d\theta}{dt} \right]. \quad (18)$$

Substituting Equation 16 into Equation 18, the acceleration of the multilayer shear zone with localization is

$$\frac{dV}{dt} = \begin{cases} A_0 \left\{ \frac{1}{A_0} \frac{dN}{dt} \frac{V}{N} + \beta N \left( \frac{V}{V_{th}N} + 1 \right)^2 \left[ 1 - \left( \frac{V}{V_{th}N} + 1 \right)^{-\frac{\beta-1}{\beta}} \right] \right\} \text{ (Aging law),} \\ A_0 \left[ \frac{1}{A_0} \frac{dN}{dt} \frac{V}{N} + (\beta - 1) N \left( \frac{V}{V_{th}N} + 1 \right)^2 \ln \left( \frac{V}{V_{th}N} + 1 \right) \right] \text{ (Slip law),} \end{cases} \quad (19)$$

where  $dN/dt$  represents the time evolution of  $N$ . When  $N = 1$  and  $dN/dt = 0$ , Equation 19 returns to Equation 11, the “single slip surface” model.

The localization of a shear zone generally suggests a reduction in active thickness with displacement (Hull, 1988; Vitale & Mazzoli, 2008). Experiments with granular material reveal an initial phase of distributed, flow-like shear, which then localizes onto a limited thickness or one single slip plane (Fukuoka et al., 2006; Haines et al., 2013; Rathbun & Marone, 2010; Tchalenko, 1970). Specifically, Chang et al. (2024) show structural evolution from multiple discontinuous shear planes to a single, highly localized plane in analog granular systems, though a quantitative description of shear localization dynamics is still lacking. In the accelerating creep scenario, slip displacement initially increases very slowly and then accelerates. Consequently,  $N$  may decay slowly at first, then decrease rapidly, and finally approach 1 asymptotically as shear localization completes. To capture this behavior, we introduce a time-dependent logistic model to describe  $N$ , potentially offering a novel approximation of the localization phenomena. The equation reads

$$N(t) = \frac{(N_0 - N_\infty)[1 + \exp(-kt_*)]}{1 + \exp[k(t - t_*)]} + N_\infty, \quad (20)$$

where  $N_0$  and  $N_\infty$  are the initial and asymptotic values of  $N$  respectively,  $k$  describes the decay rate, and  $t_*$  is the characteristic time at which maximum decay rate occurs. We set  $N_\infty = 1$  to represent the final single slip surface and use  $t_0 = L/V_{th}$  to denote a time scale. Thus, shear localization is simplified to continuous decreases in  $N$  to 1 with nondimensional time  $t/t_0$ , as depicted in Figure 5a.

We set initial  $V = 10^{-5}$  mm/s, which is typical for our experiments (Figure 2), and arbitrarily select a  $k$  value that satisfies the definition of accelerating creep, where  $dV/dt > 0$ . To model substantial localization, we use a large  $N_0$  but vary  $t_*/t_0$  (Figures 5b and 5c). Both the aging law and slip law exhibit evident slow and fast regimes, characterized by  $\alpha \approx 1$  and 2, respectively. Initially setting  $t_*/t_0$  to approximate  $V \approx V_{th}$  shows a dip near the point of rapid localization (Figure 5b), similar to samples undergoing first-time shear (Figure 2a). In contrast, a larger  $t_*/t_0$  results in a less distinct dip (Figure 4c). Furthermore, we use  $N = 1$  to model a pre-sheared sample (Figure 4d). Consequently, the transition is continuous.

## 5. Interpretation, Implications, and Limitations

The observed slow-to-fast transition in slip displacement, characterized by two distinct acceleration regimes with an evolving  $\alpha$  from approximately 1 to 2 (Figure 2), aligns well with diverse measurements in natural events, such as landslides (e.g., Hayashi & Yamamori, 1991; D. Petley and Petley, 2006) and volcanic eruptions (e.g., Kilburn, 2003; McGuire & Kilburn, 1997). The single slip surface model (Equation 11) effectively describes this dynamic transition behavior, where the evolution of  $\alpha$  is attributed to a shift in surface frictional properties, from

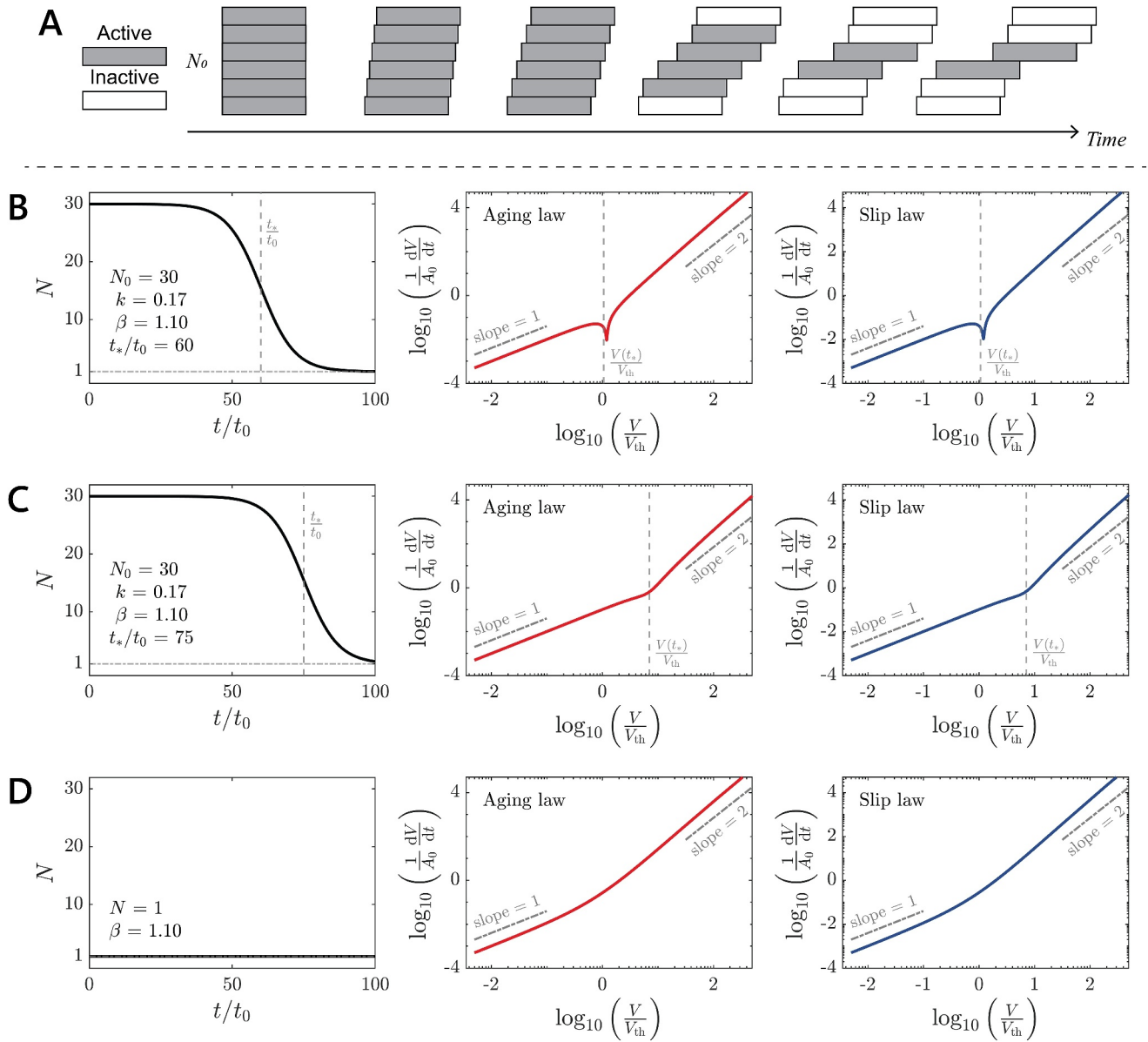


**Figure 5.** Schematic of idealized shear localization (a). Nondimensional acceleration versus nondimensional velocity for  $t_*/t_0 = 60$  (b) and 75 (c), and  $N = 1$  (d), for various shear localization processes (Dashed lines with slopes of 1 and 2 serve as guides to the eye).

velocity-independent to velocity-weakening (Figure 4). Fundamentally, this transition in accelerating creep occurs when  $V = V_{th}$  in a shear system with a single slip surface and remains valid under relatively constant loading conditions, irrespective of the geological context or frictional parameter.

However, the single slip surface model may be an oversimplification, as structural evolution and thick shear zones observed in our experiments (Figure 3b) are ubiquitously found in earthquake faults (e.g., Chambon et al., 2006; Engelder, 1974; Robertson, 1982; Scholz, 1987) and landslides (e.g., Davies et al., 1999; Davies & McSaveney, 2002, 2009; Fleming & Johnson, 1989; Schulz et al., 2017). To address this, a multilayer structure (Figure 5a) may provide a useful first-order approximation for modeling shear localization (Figure 3b).

In our numerical modeling, rapid localization causes the dip during the slow-to-fast transition (Figure 5b) due to the negative first term in Equation 19, where  $dN/dt < 0$ , which reduces acceleration. Importantly, the dip observed in this model (Figure 5b) qualitatively reproduces experimental features (Figure 2a), suggesting that the characteristic time  $t_*$  for rapid localization may not be an independent parameter. Namely, substantial localization

may tend to coincide with the slow-to-fast transition around  $V \approx V_{th}$ , when  $-df_{ss}/d \ln(V)$  (Equation 7) becomes sufficiently large, that is, when velocity-weakening becomes significant.

An immature shear zone, characterized by a large  $N_0$ , likely exhibits a prolonged slow regime because velocity  $V/N$  for each layer tends to be smaller than  $V_{th}$  (Figures 5b and 5c). Once shear localization is well-established, such as in a pre-existing shear zone with significantly smaller absolute values of  $N$  and  $dN/dt$ , the transition becomes continuous (Figures 2b and 5d), and the variabilities of  $\delta_A$  may decrease (Figure 3a). This role of deformation history is reminiscent of increases in  $\alpha$  observed in successive events at the same landslides (Crosta & Agliardi, 2003; D. Petley and Petley, 2006). Additionally, significantly smaller  $\alpha < 1$  observed in slopes with artificial reinforcement (Bozzano et al., 2014) suggests the influence of structural factors.

Acceleration characterized by  $\alpha = 1$  indicates a logarithmic increase in velocity over time, which is less catastrophic compared to power-law acceleration with a larger  $\alpha$ . Notably, many clay-rich, slow-moving landslides rarely exhibit catastrophic acceleration (e.g., Keefer & Johnson, 1983; Schulz et al., 2017). Laboratory results often reveal that velocity-strengthening of samples is negligible, hence insufficient to explain this lack of catastrophic acceleration (e.g., Keefer & Johnson, 1983; Skempton, 1985; van Asch et al., 2007). Our theoretical analysis suggests that “slow” slip instability is likely driven by velocity-independent frictional properties (Figure 4). Additionally, our numerical model indicates that the multilayer structure and shear localization processes can further moderate slow slips, resulting in transient, subtle acceleration (Figure 5).

However, our analysis does not address the final instability that occurs when acceleration is sufficiently large, potentially disrupting the quasi-static assumption and allowing other significant dynamic weakening mechanisms to take effect. Additionally, our models omit factors such as rheology or internal deformation of the landslide body (e.g., spreading due to lateral extension or liquefaction), and variable loading conditions (e.g., pore pressure fluctuations or external load). Furthermore, more sophisticated models are needed to capture the critical shear behavior of granular material in response to pore pressure change (e.g., Chang & Wang, 2022; Iverson et al., 2000; Schulz et al., 2009), dilation-induced strengthening mechanisms (e.g., Segall et al., 2010; Segall & Rice, 1995), and shear localization dynamics (e.g., Chang et al., 2024; Walley, 2007), in order to bridge the gap between our theoretical analysis and experimental observations.

## 6. Conclusions

Fluid-injection creep experiments on clayey soil show two distinct acceleration regimes with a shear-history-dependent dynamic transition, characterized by power-law velocity-acceleration relationships with exponents evolving from 1 to 2. This observation aligns with measurements of natural instabilities across various geological settings, such as landslides and volcanic eruptions. Using a single slip surface model governed by regularized rate-and-state friction in constant-load creep tests, we describe the continuous slow-to-fast transition as driven by a shift from velocity-independent to velocity-weakening steady-state friction—a mechanism potentially applicable across various clayey soils. By incorporating idealized shear localization based on observed multilayer structures in experimental shear zones, we qualitatively assess the impact of structural evolution on this history-dependent transition. These findings highlight how the combined effects of frictional properties and structural evolution can modulate slow and fast slip instabilities in natural shear systems.

## Data Availability Statement

The complete experimental dataset is available in Chang (2024).

## References

- Andrés, S., Santillán, D., Mosquera, J. C., & Cueto-Felgueroso, L. (2019). Delayed weakening and reactivation of rate-and-state faults driven by pressure changes due to fluid injection. *Journal of Geophysical Research: Solid Earth*, *124*(11), 11917–11937. <https://doi.org/10.1029/2019JB018109>
- Bozzano, F., Cipriani, I., Mazzanti, P., & Prestinanzi, A. (2014). A field experiment for calibrating landslide time-of-failure prediction functions. *International Journal of Rock Mechanics and Mining Sciences*, *67*, 69–77. <https://doi.org/10.1016/j.ijrmms.2013.12.006>
- Chambon, G., Schmittbuhl, J., Corfdir, A., Orellana, N., Diraison, M., & Géraud, Y. (2006). The thickness of faults: From laboratory experiments to field scale observations. *Tectonophysics*, *426*(1–2), 77–94. <https://doi.org/10.1016/j.tecto.2006.02.014>
- Chang, C. (2024). Supplemental material for slow-to-fast transition and shear localization in accelerating creep of clayey soil [Dataset]. *Zenodo*. <https://doi.org/10.5281/zenodo.11513623>
- Chang, C., Noda, H., Hamada, Y., Huang, C., Ma, T., Wang, G., & Yamaguchi, T. (2024). Comminution-induced transient frictional behavior in sheared granular halite. *Geophysical Research Letters*, *51*(21), e2024GL109645. <https://doi.org/10.1029/2024GL109645>

## Acknowledgments

We are very grateful for the constructive feedback from the reviewers and editors. We also thank Huihui Weng, Will Steinhardt, Changrong He, and Lu Yao for stimulating discussions, Chao Huang for helpful assistance, and Carlisle Landel for insightful editing. We gratefully acknowledge support from JSPS KAKENHI (No. JP21H05201, “Science of Slow to Fast Earthquakes”) and the SKLGP Open Fund (No. 2024K033, “The Physics of Empirical Models for Landslide Failure-time Prediction”).

- Chang, C., & Wang, G. (2022). Creep of clayey soil induced by elevated pore-water pressure: Implication for forecasting the time of failure of rainfall-triggered landslides. *Engineering Geology*, 296, 106461. <https://doi.org/10.1016/j.enggeo.2021.106461>
- Crosta, G. B., & Agliardi, F. (2003). Failure forecast for large rock slides by surface displacement measurements. *Canadian Geotechnical Journal*, 40(1), 176–191. <https://doi.org/10.1139/02-085>
- Davies, T. R., & McSaveney, M. J. (2002). Dynamic simulation of the motion of fragmenting rock avalanches. *Canadian Geotechnical Journal*, 39(4), 789–798. <https://doi.org/10.1139/02-035>
- Davies, T. R., & McSaveney, M. J. (2009). The role of rock fragmentation in the motion of large landslides. *Engineering Geology*, 109(1–2), 67–79. <https://doi.org/10.1016/j.enggeo.2008.11.004>
- Davies, T. R., McSaveney, M. J., & Hodgson, K. A. (1999). A fragmentation-spreading model for long-runout rock avalanches. *Canadian Geotechnical Journal*, 36(6), 1096–1110. <https://doi.org/10.1139/99-067>
- Dieterich, J. H. (1979). Modeling of rock friction: 1. Experimental results and constitutive equations. *Journal of Geophysical Research*, 84(B5), 2161–2168. <https://doi.org/10.1029/JB084iB05p02161>
- Drysdale, W. H. (1984). *A theory of rate-dependent plasticity*. Defense Technical Information Center. <https://doi.org/10.21236/ADA142102>
- Drysdale, W. H., & Zak, A. R. (1985). A theory for rate-dependent plasticity. *Computers and Structures*, 20(1), 259–264. [https://doi.org/10.1016/0045-7949\(85\)90075-6](https://doi.org/10.1016/0045-7949(85)90075-6)
- Engelder, J. T. (1974). Cataclasis and the generation of fault gouge. *The Geological Society of America Bulletin*, 85(10), 1515. [https://doi.org/10.1130/0016-7606\(1974\)85<1515:CATGOF>2.0.CO;2](https://doi.org/10.1130/0016-7606(1974)85<1515:CATGOF>2.0.CO;2)
- Federico, A., Popescu, M., Elia, G., Fidelibus, C., Internò, G., & Murianni, A. (2012). Prediction of time to slope failure: A general framework. *Environmental Earth Sciences*, 66(1), 245–256. <https://doi.org/10.1007/s12665-011-1231-5>
- Ferri, F., Di Toro, G., Hirose, T., Han, R., Noda, H., Shimamoto, T., et al. (2011). Low-to high-velocity frictional properties of the clay-rich gouges from the slipping zone of the 1963 Vaiont slide, northern Italy. *Journal of Geophysical Research*, 116(B9), B09208. <https://doi.org/10.1029/2011JB008338>
- Fleming, R. W., & Johnson, A. M. (1989). Structures associated with strike-slip faults that bound landslide elements. *Engineering Geology*, 27(1), 39–114. [https://doi.org/10.1016/0013-7952\(89\)90031-8](https://doi.org/10.1016/0013-7952(89)90031-8)
- Fukuoka, H., Sassa, K., Wang, G., & Sasaki, R. (2006). Observation of shear zone development in ring-shear apparatus with a transparent shear box. *Landslides*, 3(3), 239–251. <https://doi.org/10.1007/s10346-006-0043-2>
- Fukuzono, T. F. (1985). A new method for predicting the failure time of a slope. *Proceedings of 4<sup>th</sup> International Conference and Field Workshop on Landslide, 1985*, 145–150. Retrieved from <https://cir.nii.ac.jp/crid/1574231874803735936>
- Haines, S. H., Kaproth, B., Marone, C., Saffer, D., & van der Pluijm, B. (2013). Shear zones in clay-rich fault gouge: A laboratory study of fabric development and evolution. *Journal of Structural Geology*, 51, 206–225. <https://doi.org/10.1016/j.jsg.2013.01.002>
- Hayashi, S., & Yamamori, T. (1991). Basic equation of slide in tertiary creep and features of its parameters. *Journal of Japan Landslide Society*, 28(1), 17–22. <https://doi.org/10.3313/jls1964.28.17>
- Heap, M. J., Baud, P., Meredith, P. G., Vinciguerra, S., Bell, A. F., & Main, I. G. (2011). Brittle creep in basalt and its application to time-dependent volcano deformation. *Earth and Planetary Science Letters*, 307(1–2), 71–82. <https://doi.org/10.1016/j.epsl.2011.04.035>
- Helmstetter, A., Sornette, D., Grasso, J.-R., Andersen, J. V., Gluzman, S., & Pisarenko, V. (2004). Slider block friction model for landslides: Application to Vaiont and La Clapière landslides. *Journal of Geophysical Research*, 109(B2). <https://doi.org/10.1029/2002JB002160>
- Hull, J. (1988). Thickness-displacement relationships for deformation zones. *Journal of Structural Geology*, 10(4), 431–435. [https://doi.org/10.1016/0191-8141\(88\)90020-X](https://doi.org/10.1016/0191-8141(88)90020-X)
- Intrieri, E., Carlà, T., & Gigli, G. (2019). Forecasting the time of failure of landslides at slope-scale: A literature review. *Earth-Science Reviews*, 193, 333–349. <https://doi.org/10.1016/j.earscirev.2019.03.019>
- Iverson, R. M., Reid, M. E., Iverson, N. R., LaHusen, R. G., Logan, M., Mann, J. E., & Brien, D. L. (2000). Acute sensitivity of landslide rates to initial soil porosity. *Science*, 290(5491), 513–516. <https://doi.org/10.1126/science.290.5491.513>
- Keefer, D. K., & Johnson, A. M. (1983). *Earth flows: Morphology, mobilization, and movement*. U.S. Geological Survey Professional Paper. <https://doi.org/10.3133/pp1264>
- Kilburn, C. R. J. (2003). Multiscale fracturing as a key to forecasting volcanic eruptions. *Journal of Volcanology and Geothermal Research*, 125(3–4), 271–289. [https://doi.org/10.1016/S0377-0273\(03\)00117-3](https://doi.org/10.1016/S0377-0273(03)00117-3)
- Main, I. G. (1999). Applicability of time-to-failure analysis to accelerated strain before earthquakes and volcanic eruptions. *Geophysical Journal International*, 139(3), F1–F6. <https://doi.org/10.1046/j.1365-246x.1999.00004.x>
- Marone, C. (1998). Laboratory-derived friction laws and their application to seismic faulting. *Annual Review of Earth and Planetary Sciences*, 26(1), 643–696. <https://doi.org/10.1146/annurev.earth.26.1.643>
- McGuire, W. J., & Kilburn, C. R. J. (1997). Forecasting volcanic events: Some contemporary issues. *Geologische Rundschau*, 86(2), 439–445. <https://doi.org/10.1007/s005310050152>
- Noda, H., & Chang, C. (2023). Tertiary creep behavior for various rate- and state-dependent friction laws. *Earth and Planetary Science Letters*, 619, 118314. <https://doi.org/10.1016/j.epsl.2023.118314>
- Paul, K., Bhattacharya, P., & Misra, S. (2024). Frictional control on accelerating creep during the slow-to-fast transition of rainfall-induced catastrophic landslides. *Journal of Geophysical Research: Earth Surface*, 129(1), e2023JF007213. <https://doi.org/10.1029/2023JF007213>
- Petley, D. N., Bulmer, M. H., & Murphy, W. (2002). Patterns of movement in rotational and translational landslides. *Geology*, 30(8), 719. [https://doi.org/10.1130/0091-7613\(2002\)030<0719:POMIRA>2.0.CO;2](https://doi.org/10.1130/0091-7613(2002)030<0719:POMIRA>2.0.CO;2)
- Petley, D. N., & Petley, D. J. (2006). On the initiation of large rockslides: Perspectives from a new analysis of the Vaiont movement record. In S. G. Evans, G. S. Mugnozza, A. Strom, & R. L. Hermanns (Eds.), *Landslides from massive rock slope failure* (Vol. 49, pp. 77–84). Springer Netherlands. [https://doi.org/10.1007/978-1-4020-4037-5\\_3](https://doi.org/10.1007/978-1-4020-4037-5_3)
- Rathbun, A. P., & Marone, C. (2010). Effect of strain localization on frictional behavior of sheared granular materials. *Journal of Geophysical Research*, 115(B1), B01204. <https://doi.org/10.1029/2009JB006466>
- Robertson, E. C. (1982). Continuous Formation of gouge and breccia during fault displacement. In *Presented at the the 23rd U.S symposium on rock mechanics (USRMS)*. OnePetro. Retrieved from <https://onepetro.org/ARMAUSRMS/proceedings-abstract/ARMA82/AII-ARMA82/129291>
- Rose, N. D., & Hungr, O. (2007). Forecasting potential rock slope failure in open pit mines using the inverse-velocity method. *International Journal of Rock Mechanics and Mining Sciences*, 44(2), 308–320. <https://doi.org/10.1016/j.ijrmms.2006.07.014>
- Ruina, A. (1983). Slip instability and state variable friction laws. *Journal of Geophysical Research*, 88(B12), 10359–10370. <https://doi.org/10.1029/JB088iB12p10359>
- Scaringi, G., & Di Maio, C. (2016). Influence of displacement rate on residual shear strength of clays. *Procedia Earth and Planetary Science*, 16, 137–145. <https://doi.org/10.1016/j.proeps.2016.10.015>

- Scaringi, G., Hu, W., Xu, Q., & Huang, R. (2018). Shear-rate-dependent behavior of clayey bimaterial interfaces at landslide stress levels. *Geophysical Research Letters*, *45*(2), 766–777. <https://doi.org/10.1002/2017GL076214>
- Scholz, C. H. (1987). Wear and gouge formation in brittle faulting. *Geology*, *15*(6), 493. [https://doi.org/10.1130/0091-7613\(1987\)15<493:WAGFIB>2.0.CO;2](https://doi.org/10.1130/0091-7613(1987)15<493:WAGFIB>2.0.CO;2)
- Schulz, W. H., Coe, J. A., Ricci, P. P., Smoczyk, G. M., Shurtleff, B. L., & Panosky, J. (2017). Landslide kinematics and their potential controls from hourly to decadal timescales: Insights from integrating ground-based InSAR measurements with structural maps and long-term monitoring data. *Geomorphology*, *285*, 121–136. <https://doi.org/10.1016/j.geomorph.2017.02.011>
- Schulz, W. H., McKenna, J. P., Kibler, J. D., & Biavati, G. (2009). Relations between hydrology and velocity of a continuously moving landslide—Evidence of pore-pressure feedback regulating landslide motion? *Landslides*, *6*(3), 181–190. <https://doi.org/10.1007/s10346-009-0157-4>
- Segalini, A., Valletta, A., & Carri, A. (2018). Landslide time-of-failure forecast and alert threshold assessment: A generalized criterion. *Engineering Geology*, *245*, 72–80. <https://doi.org/10.1016/j.enggeo.2018.08.003>
- Segall, P., & Rice, J. R. (1995). Dilatancy, compaction, and slip instability of a fluid-infiltrated fault. *Journal of Geophysical Research*, *100*(B11), 22155–22171. <https://doi.org/10.1029/95JB02403>
- Segall, P., Rubin, A. M., Bradley, A. M., & Rice, J. R. (2010). Dilatant strengthening as a mechanism for slow slip events. *Journal of Geophysical Research*, *115*(B12). <https://doi.org/10.1029/2010JB007449>
- Skempton, A. W. (1985). Residual strength of clays in landslides, folded strata and the laboratory. *Géotechnique*, *35*(1), 3–18. <https://doi.org/10.1680/geot.1985.35.1.3>
- Sornette, D., Helmstetter, A., Andersen, J. V., Gluzman, S., Grasso, J.-R., & Pisarenko, V. (2004). Towards landslide predictions: Two case studies. *Physica A: Statistical Mechanics and its Applications*, *338*(3–4), 605–632. <https://doi.org/10.1016/j.physa.2004.02.065>
- Tal, Y., Hager, B. H., & Ampuero, J. P. (2018). The effects of fault roughness on the earthquake nucleation process. *Journal of Geophysical Research: Solid Earth*, *123*(1), 437–456. <https://doi.org/10.1002/2017JB014746>
- Tchalenko, J. S. (1970). Similarities between shear zones of different magnitudes. *The Geological Society of America Bulletin*, *81*(6), 1625. [https://doi.org/10.1130/0016-7606\(1970\)81\[1625:SBSZOD\]2.0.CO;2](https://doi.org/10.1130/0016-7606(1970)81[1625:SBSZOD]2.0.CO;2)
- Tepp, G., Hotovec-Ellis, A., Shiro, B., Johanson, I., Thelen, W., & Haney, M. M. (2020). Seismic and geodetic progression of the 2018 summit caldera collapse of Kīlauea volcano. *Earth and Planetary Science Letters*, *540*, 116250. <https://doi.org/10.1016/j.epsl.2020.116250>
- Tika, T. E., Vaughan, P. R., & Lemos, L. J. L. J. (1996). Fast shearing of pre-existing shear zones in soil. *Géotechnique*, *46*(2), 197–233. <https://doi.org/10.1680/geot.1996.46.2.197>
- van Asch, T. W. J., Van Beek, L. P. H., & Bogaard, T. A. (2007). Problems in predicting the mobility of slow-moving landslides. *Engineering Geology*, *91*(1), 46–55. <https://doi.org/10.1016/j.enggeo.2006.12.012>
- Vitale, S., & Mazzoli, S. (2008). Heterogeneous shear zone evolution: The role of shear strain hardening/softening. *Journal of Structural Geology*, *30*(11), 1383–1395. <https://doi.org/10.1016/j.jsg.2008.07.006>
- Voight, B. (1988). A method for prediction of volcanic eruptions. *Nature*, *332*(6160), 125–130. <https://doi.org/10.1038/332125a0>
- Voight, B. (1989). A relation to describe rate-dependent material failure. *Science*, *243*(4888), 200–203. <https://doi.org/10.1126/science.243.4888.200>
- Walley, S. M. (2007). Shear localization: A historical overview. *Metallurgical and Materials Transactions A*, *38*(11), 2629–2654. <https://doi.org/10.1007/s11661-007-9271-x>
- Xue, J., Hao, S., Wang, J., Ke, F., Lu, C., & Bai, Y. (2018). The changeable power law singularity and its application to prediction of catastrophic rupture in uniaxial compressive tests of geomedia. *Journal of Geophysical Research: Solid Earth*, *123*(4), 2645–2657. <https://doi.org/10.1002/2018JB015591>
- Yang, Z., Zhang, H. P., & Marder, M. (2008). Dynamics of static friction between steel and silicon. *Proceedings of the National Academy of Sciences*, *105*(36), 13264–13268. <https://doi.org/10.1073/pnas.0806174105>

## References From the Supporting Information

- Sassa, K., Fukuoka, H., Wang, G., & Ishikawa, N. (2004). Undrained dynamic-loading ring-shear apparatus and its application to landslide dynamics. *Landslides*, *1*, 7–19. <https://doi.org/10.1007/s10346-003-0004-y>
- Szatmari, A. (2024). SmithWatermanMorphing [Software]. *GitHub*. <https://github.com/szat/SmithWatermanMorphing>
- Jiang, X., Bunke, H., Abegglen, K., & Kandel, A. (2002). Curve morphing by weighted mean of strings. In *Proceedings of the international conference on pattern recognition (ICPR)* (Vol. 4, pp. 192–195). IEEE. <https://doi.org/10.1109/ICPR.2002.1047430>